

# Subthreshold Antiproton Spectra in Relativistic Heavy Ion Collisions

Richard Wittmann and Ulrich Heinz

*Institut für Theoretische Physik, Universität Regensburg,*

*D-93040 Regensburg, Germany*

(October 2, 2018)

## Abstract

We study the structure of antiproton spectra at extreme subthreshold bombarding energies using a thermodynamic picture. Antiproton production processes and final state interactions are discussed in detail in order to find out what can be learned about these processes from the observed spectra.

## I. INTRODUCTION

There exist numerous examples for the production of particles in heavy ion collisions at bombarding energies well below the single nucleon-nucleon threshold [1]. This phenomenon indicates collective interactions among the many participating nucleons and thus is expected to give information about the hot and dense matter formed in these collisions. At beam energies around 1 GeV per nucleon the most extreme of these subthreshold particles is the antiproton. Therefore, it is believed to be a very sensitive probe to collective behaviour in nucleus-nucleus collisions.

However, presently neither the production mechanism nor the final state interactions of antiprotons in dense nucleonic matter are well understood. The antiproton yields measured at GSI and BEVALAC [2,3] seem to be described equally well by various microscopic models using different assumptions about the production mechanism and particle properties in dense nuclear matter [4–7]. This ambiguity raises the question which kind of information can be really deduced from subthreshold  $\bar{p}$  spectra. In this paper we use a simple thermodynamic framework as a background on which we can systematically study the influence of different assumptions on the final  $\bar{p}$  spectrum.

In the next section we will focus on the production process. Following a discussion of the final state interactions of the antiproton in dense hadronic matter in Section III, we use in Section IV a one-dimensional hydrodynamic model for the exploding fireball to clarify which features of the production and reabsorption mechanisms should survive in the final spectra in a dynamical environment. We summarize our results in Section V.

## II. PRODUCTION OF ANTIPROTONS IN HEAVY ION COLLISIONS

### A. The Antiproton Production Rate

Unfortunately very little is known about the production mechanism for antiprotons in dense nuclear matter. Therefore, we are forced to use intuitive arguments to obtain a

plausible expression for the production rate. As commonly done in microscopic models [8] we consider only two body collisions and take the experimentally measured cross sections for  $\bar{p}$  production in free NN collisions as input. The problem can then be split into two parts: the distribution of the two colliding nucleons in momentum space and the elementary cross sections for antiproton production. The procedure is later generalized to collisions among other types of particles (Section II C) using phase space arguments. Formally, the antiproton production rate  $P$ , i.e. the number of antiprotons produced in the space-time cell  $d^4x$  and momentum space element  $d^3p$ , is given by [9]

$$P = \sum_{i,j} \int ds 2 w(s) \frac{d^3\sigma_{ij \rightarrow \bar{p}}(s)}{d^3p} \int d\omega_i d\omega_j \delta(s - (p_i + p_j)^2) f_i f_j. \quad (1)$$

In this expression the summation includes all incoming particle species  $i$  and  $j$  with 4-momenta  $p_i$  and  $p_j$  and phase space distributions  $f_i$  and  $f_j$ , respectively. The integration is over the invariant collision energy  $s = (p_i + p_j)^2$  and the phase space of the two colliding particles:

$$d\omega_i \equiv \frac{d^4p_i}{(2\pi)^3} \delta(p_i^2 - m_i^2) \Theta(p_i^0). \quad (2)$$

Finally,  $w(s, m_i, m_j) = \sqrt{(s - (m_i - m_j)^2)(s - (m_i + m_j)^2)}$  is the well known flux factor, and  $d^3\sigma_{ij \rightarrow \bar{p}}(s)/d^3p$  the differential  $\bar{p}$  production cross section. The influence of the shape of the phase space distributions and of the differential production cross sections will now be investigated in more detail, beginning with the case of  $\bar{p}$  production by  $NN$  collisions.

## B. Phase Space Distributions and Parametrisation of the Differential Production Cross Sections

Assuming that the momentum distribution of the nucleons gradually evolves from  $\delta$ -peaks at the momenta of the colliding nuclei to a relativistic Maxwell-Boltzmann distribution, an analytical expression for the phase space distribution  $f_{i,j}$  was derived by Schürmann *et al.* in Ref. [10]. We use this model as the basis for a numerical evaluation of the probability  $\lambda(s, t)$

of finding two nucleons at a center-of-mass energy  $\sqrt{s}$  at time  $t$  (the second integral on the right hand side of Eq. (1)). Fig. 1 shows  $\lambda(s, t)$  at  $t = 0.2, 2, 5$  fm/c after the nuclei have started overlapping, assuming a bombarding energy of 1 GeV/A. Although the initial  $\delta$ -like distribution at  $s = 5.5 \text{ GeV}^2$  widens quite rapidly, the extreme states needed for antiproton production ( $s \geq (4m)^2 = 14.1 \text{ GeV}^2$ ) are populated substantially only after about 5 fm/c. At this moment the distribution is already nearly a relativistic Maxwell-Boltzmann distribution (dashed line) which maximizes the  $\bar{p}$  production rate in our approach. This fact motivates us to neglect pre-equilibrium production and to switch on  $\bar{p}$ -production only when the system has reached local thermal equilibrium. Similiar conclusions have been drawn from the results of a microscopic kinetic model for the phase space evolution [4]. There it was demonstrated that only nucleons which have suffered at least several collisions are effective in  $\bar{p}$  production.

There are no experimental data for the nucleonic processes

$$p + p \rightarrow p + p + p + \bar{p}$$

$$n + p \rightarrow n + p + p + \bar{p}$$

close to the production threshold. As already pointed out in [11], different extrapolations of the data at higher energies down to threshold change the  $\bar{p}$ -yield by orders of magnitude. However, we will show that not only the total yield, but also the shape of the spectrum is very sensitive to the threshold behaviour. We choose for the production cross section the parametrization

$$\sigma(s) = \sigma_0 \frac{(\sqrt{s} - 4m)^\alpha}{w^2(s)}, \quad (3)$$

where the parameter  $\alpha$  models the shape of the cross section near threshold. The normalization  $\sigma_0$  is determined by the experimentally measured point closest to threshold. If the behaviour of  $\sigma(s)$  were dominated by the available phase space for the outgoing particles (this is the fundamental assumption in Fermi's statistical model [12]), then  $\alpha = 7/2$ .

In order to obtain from the total cross section (3) a formula for the differential cross section, we assume like others that the momentum distribution of the produced particles is mainly governed by phase space. This leads to the simple relationship

$$\frac{d^3\sigma_{ij\rightarrow NNN\bar{p}}(s)}{d^3p} \sim \frac{R_3(P - p_{\bar{p}})}{R_4(P)} \sigma_{ij\rightarrow NNN\bar{p}}(s). \quad (4)$$

Here  $R_n$  is the volume the  $n$ -particle phase space, which can be given analytically in the non-relativistic limit [12].  $P$  is the total 4-momentum of the 4-particle final state, which reduces to  $(\sqrt{s}, 0)$  in the CMS of the four particles.

Inserting (3) and (4) into (1) and using thermal phase space distributions, the production spectrum can be evaluated numerically. As seen in Fig. 2, the sensitivity on the threshold power  $\alpha$  is particularly pronounced for low-energy antiprotons. The strong deviation at low  $\bar{p}$  energies from a thermal shape (dashed lines) for small values of  $\alpha$  is most remarkable.

Using the Fermi value  $\alpha = 7/2$  for the cross section, an analytical expression for the production rate can be obtained:

$$P \sim \rho_i \rho_j e^{-\sqrt{s_{\min}(p)}/T}.$$

Here  $\rho_{i,j}$  are the densities of the incoming particles,  $\sqrt{s_{\min}(p)}$  is the threshold for producing an antiproton with momentum  $p$ , and  $T$  is the local temperature of the environment. Clearly the rate  $P$  is proportional to the product of the densities of the two colliding particle species  $i$  and  $j$ . More importantly, this formula shows the extreme sensitivity on the production threshold and on the medium temperature which both appear in the exponent of the exponential function.

### C. Production by Resonances and Mesons

The production of resonances as intermediate energy storage has been pointed out as an important mechanism for  $\bar{p}$  production in [14]. Because no experimental data are available for antiproton production by baryonic resonances, we follow common strategy [14] and assume

that the cross section  $\sigma_{ij \rightarrow NNN\bar{p}}(s)$  is independent of the internal state of excitation of the colliding baryons in our thermal picture. The consequences of this assumption are quite obvious. While the distance to the  $\bar{p}$ -threshold is reduced by the larger rest mass of the resonances, the mean velocity of a heavy resonance state in a thermal system is smaller than that of a nucleon. Both factors counteract each other, and indeed we found that the total rate  $P$  is not strongly changed by the inclusion of resonances.

The role of pionic intermediate states for  $\bar{p}$ -production in  $pp$ -collisions was pointed out by Feldman [15]. As mesons are created numerously in the course of a heavy ion collision, mesonic states gain even more importance in this case. In fact, Ko and Ge [13] claimed that  $\rho\rho \rightarrow p\bar{p}$  should be the dominant production channel. Relating the  $\rho\rho$ -production channel to the  $p\bar{p}$  annihilation channel [13] by

$$\sigma_{\rho\rho \rightarrow p\bar{p}}(s) = \left(\frac{2}{2S+1}\right)^2 \left(\frac{s-4m}{s-4m_\rho}m\right) \sigma_{p\bar{p} \rightarrow \rho\rho}(s) \quad (5)$$

where  $S = 1$  is the spin factor for the  $\rho$ , the production rate can be calculated straightforwardly from Eq. (1):

$$P = \frac{g_\rho^2}{6} \frac{\pi T}{(2\pi)^5} \frac{16}{9\pi} w(4E^2, m, m) \sigma_{p\bar{p} \rightarrow \rho\rho}(4E^2) K_1\left(\frac{2E}{T}\right). \quad (6)$$

The spin-isospin factor of the  $\rho$  is  $g_\rho = 9$ , and  $E$  is the energy of the produced antiproton. The modified Bessel function  $K_1$  results from the assumption of local thermal equilibration for the  $\rho$ -distribution. Expanding the Bessel function for large values of  $2E/T$  we see that the "temperature"  $T_{\bar{p}}$  of the  $\bar{p}$ -spectrum is only half the medium temperature:  $T_{\bar{p}} = \frac{1}{2}T$ .

Finally, the meson-baryon collision process

$$m_i + B_j \rightarrow B_k + p + \bar{p} \quad (7)$$

remains as the last prototype of collisions with two incoming particles. We choose a parametrisation for the cross section which reflects its qualitative behaviour [14]:

$$\sigma(ij \rightarrow NNN\bar{p})(s) = \sigma_{ij}^0 s_0 \frac{s - s_0}{w^2(s, m_i, m_j)} \quad (8)$$

Comparing this form with measured data on  $\pi^-p \rightarrow np\bar{p}$  collisions [16], a value of  $\sigma_{ij}^0 = 0.35$  mb is obtained. Due to the threshold behaviour of Eq. (8) and the rather large value of  $\sigma_{ij}^0$ , it turns out [17] that this process is by far the most important one in a *chemically* equilibrated system. However, this chemical equilibration – if achieved at all – is reached only in the final stages of the heavy ion collision when cooling has already started. So it is by no means clear whether the dominance of the meson-baryon channel remains valid in a realistic collision scenario. This point will be further discussed in Section IV.

### III. FINAL STATE INTERACTION OF THE ANTIPROTON

Once an antiproton is created in the hot and dense hadronic medium, its state will be modified by interactions with the surrounding particles. Two fundamentally different cases have to be distinguished: elastic scattering, which leads to a reconfiguration in phase space, driving the momentum distribution towards a thermal one with the temperature of the surrounding medium, and annihilation. Each process will be considered in turn.

#### A. Elastic Scattering

The time evolution of the distribution function  $f(p, t)$  is generally described by the equation [18]

$$f(p, t_2) = \int w(p, p'; t_2, t_1) f(p', t_1) dp' \quad (9)$$

where  $w(p, p'; t_2, t_1)$  is the transition probability from momentum state  $p'$  at time  $t_1$  to state  $p$  at  $t_2$ . Because the number density of antiprotons is negligible compared to the total particle density in the system, the evolution of  $f(p, t)$  can be viewed as a Markov process. Assuming furthermore that the duration of a single scattering process  $\tau$  and the mean free path  $\lambda$  are small compared to the typical time scale  $\delta t$  and length scale  $\delta r$  which measure the variation of the thermodynamic properties of the system,

$$\tau \ll \delta t, \quad \lambda \ll \delta r,$$

Eq. (9) can be transformed into a master equation. Considering the structure of the differential  $p\bar{p}$  cross section one notices that in the interesting energy range it is strongly peaked in the forward direction [19–21]. Therefore, the master equation can be approximated by a Fokker-Planck equation [22]:

$$\frac{\partial f(p, t)}{\partial t} = -\frac{\partial}{\partial p} A(p)f(p, t) + \frac{1}{2} \frac{\partial^2}{\partial^2 p} D(p)f(p, t). \quad (10)$$

For the evaluation of the friction coefficient  $A$  and the diffusion coefficient  $D$  we follow the treatment described by Svetitsky [23]. For the differential cross section we took a form suggested in [19]:

$$\frac{d\sigma}{dt} = (b + c\lambda) \frac{J_1^2 \left[ (a + \lambda) \sqrt{|t|} \right]}{|t|}, \quad (11)$$

where the constants  $a$ ,  $b$ ,  $c$  are fitted to experimental data.  $\lambda$  is the wave number of the relative motion,  $t$  the transferred four momentum and  $J_1$  a spherical Bessel function. The essential result [17] is that the coefficients  $A$  and  $B$  are nearly independent of the  $\bar{p}$  momentum and satisfactorily fulfill the Einstein relation

$$D = m T A. \quad (12)$$

The effect of these coefficients can be visualized by examining the time evolution of a non-relativistic Maxwell-Boltzmann distribution whose initial slope  $T_0$  is different from the temperature of the medium:

$$f(p, t = 0) = N e^{-p^2/2mT_0}. \quad (13)$$

In a medium at fixed temperature  $T = 100$  MeV and normal nuclear density  $\rho_0$  the solution  $f(p, t)$  of the Fokker-Planck equation can be calculated analytically:

$$f(p, t) \sim \exp \left[ -\frac{e^{2At}}{2D/A(e^{2At} - 1) + 2mT_0} p^2 \right] \equiv \exp \left[ -p^2/2mT_{\text{eff}}(t) \right]. \quad (14)$$

This shows that the exponential shape of the distribution function is maintained throughout the time evolution, but that the slope  $T_{\text{eff}}(t)$  gradually evolves from  $T_0$  to the value  $D/mA$



which, according to the Einstein relation (12), is the medium temperature  $T$ . Looking at Fig. 3 it is clear that after about 10 fm/c the spectrum is practically thermalized. Therefore initial structures of the production spectrum (like the ones seen in Fig. 2) are washed out quite rapidly, and their experimental observation will be very difficult.

## B. Annihilation

The annihilation of antiprotons with baryons is dominated by multi-meson final states  $X$ . For the parametrisation of the annihilation cross section  $\sigma^{\text{ann}}(s)$  we take the form given in [14] for the process

$$\bar{p} + B \longrightarrow X, \quad B = N, \Delta, \dots \quad (15)$$

Using the same philosophy as for the calculation of the production rate, a simple differential equation for the decrease of the antiproton density in phase space can be written down:

$$\frac{d}{dt} \frac{d^6 N}{d^3 x d^3 p} = - \frac{d^6 N}{d^3 x d^3 p} \sum_i \int \frac{d^3 p_i}{(2\pi)^3} f_i(\vec{x}, \vec{p}_i, t) v_{i\bar{p}} \sigma_{i\bar{p}}^{\text{ann}} \equiv - \frac{d^6 N}{d^3 x d^3 p} A(\vec{x}, \vec{p}, t). \quad (16)$$

This equation shows that the absorption rate is given by the thermal average of the annihilation cross section  $A[\mu_B, T] = \langle v \sigma^{\text{ann}} \rangle$  where  $v$  is the  $\bar{p}$  velocity. Although  $\sigma^{\text{ann}}(s)$  is strongly peaked for low-energy antiprotons, the thermal average  $\langle v \sigma^{\text{ann}} \rangle$  is practically independent of the  $\bar{p}$  velocity in the medium. Therefore, in a stationary medium the shape of the  $\bar{p}$  spectrum is maintained; the momentum independence of  $A$  leads only to a renormalisation of the spectrum by annihilation. Any modifications of the spectral shape must be due to the dynamical evolution of the hadronic medium.

The absolute value of  $A$  decreases slightly with increasing temperature; it is of the order of  $0.5 \text{ (fm/c)}^{-1}$  at normal nuclear matter density. This means that 99% of the antiprotons are absorbed within 9 fm/c. Of course, due to the rather large value of the absorption rate  $A$  which is of the order of the size of the antiproton, the classical approach chosen in our model

becomes questionable. More reliable results should be based on a quantum field theoretic calculation which is beyond the scope of this paper.

## IV. ANTIPROTON SPECTRA FROM AN EXPLODING FIREBALL

### A. A Model for the Heavy Ion Collision

In order to compare the results of the two previous sections with experimental data we connect them through a dynamical model for the heavy ion reaction. In the spirit of our thermodynamic approach the so-called hadrochemical model of Montvay and Zimanyi [24] is applied for the simulation of the heavy ion collision. In this picture the reaction is split into two phases, an ignition and an explosion phase, and particles which have at least scattered once are assumed to follow a local Maxwell-Boltzmann distribution. In addition, a spherically symmetric geometry is assumed for the explosion phase. The included particle species are nucleons,  $\Delta$ -resonances, pions and  $\rho$ -mesons.

As initial condition a Fermi-type density distribution is taken for the nucleons of the incoming nuclei,

$$\rho(r) = \frac{\rho_0}{1 + e^{(r-R_0)/z}}, \quad (17)$$

with the nuclear radius  $R_0$  and a surface diffuseness  $z = 0.55$  fm. Because the Fermi motion is small compared to the typical bombarding energy of 1 GeV/A, it can be neglected, and the initial phase space distribution therefore reads

$$f(\vec{x}, \vec{p}, t) = \delta(p_x) \delta(p_y) \delta(p_z - p_0) \rho(|\vec{x} - \vec{\xi}(t)|). \quad (18)$$

Here  $\vec{\xi}(t)$  describes the path of the center of the nucleus.

Due to elastic and inelastic scattering hot and dense matter is formed in the central region. Its time-dependent chemical composition is governed by the kinetic equations of the hadrochemical model given in Ref. [24]. Their particular form needed here can be found in [17]. Some of the resulting distributions are visualized in Fig. 4 for a central  $^{40}\text{Ca}$ - $^{40}\text{Ca}$

collision with momentum  $p_z = \pm 700$  MeV in the c.m. system. One clearly sees that at the moment of full overlap of the two nuclei a dense zone with hot nucleons, resonances and mesons (not shown) has been formed. Only in the peripheral regions "cold" target and projectile nucleons can still be found. On the other hand, chemical equilibrium of the hot collision zone is not reached in the short available time before the explosion phase sets in; pions and in particular  $\rho$  mesons remain far below their equilibrium abundances [17].

It is important to note that due to the arguments given in Section II  $\bar{p}$  production is strongly suppressed in this initial stage of the reaction. In our simple model we have in fact neglected this early  $\bar{p}$  production completely. The ignition phase is only needed to obtain the chemical composition of the hot fireball which is expected to be the dominant source for the creation of antiprotons.

For the subsequent expansion of the spherically symmetric fireball into the surrounding vacuum analytical solutions can be given if the equation of state of an ideal gas is taken as input [25]. If excited states are included in the model, an exact analytical solution is no longer possible. Because a small admixture of resonances is not expected to fundamentally change the dynamics of the system, we can account for their effect in first order by adjusting only the thermodynamic parameters of the exploding fireball, but not the expansion velocity profiles.

There is one free parameter in the model [24],  $\alpha$ , which controls the density and the temperature profiles, respectively. Small values  $\alpha \rightarrow 0$  represent  $\delta$ -function like density profiles whereas  $\alpha \rightarrow \infty$  corresponds to a homogeneous density distribution throughout the fireball (square well profile). The time-dependent temperature profiles for two representative values of  $\alpha$  are shown in Fig. 5 for different times  $t$  starting at the time  $t_m$  of full overlap of the nuclei. Clearly, a small value of  $\alpha$  leads to an unreasonably high temperature ( $T \sim 200$  MeV) in the core of the fireball at the beginning of the explosion phase, and should thus be considered unphysical.

## B. Antiproton Spectra from an Exploding Fireball

Based on the time-dependent chemical composition of this hadrochemical model we can calculate the spectrum of the antiprotons created in a heavy ion collision. Let us first concentrate on the influence of the density distribution in the fireball characterized by the shape parameter  $\alpha$ . Due to different temperature profiles connected with different  $\alpha$  values (see Fig. 5) the absolute normalization varies substantially when the density profile is changed. For more  $\delta$ -like shapes an extremely hot fireball core is generated, whereas for increasing  $\alpha$  both density and temperature are more and more diffuse and spread uniformly over a wider area. Because of the exponential dependence upon temperature a small, but hot core raises the production rate drastically. This fact is illustrated in Fig. 6 for three values of  $\alpha$ . Not only the total normalization, but also the asymptotic slope of the spectrum is modified due to the variation of the core temperature with  $\alpha$  as indicated in the Figure.

Comparing the dotted lines, which give the pure production spectrum, to the solid lines representing the asymptotic spectrum at decoupling, the tremendous effect of antiproton absorption in heavy ion collisions is obvious. As one intuitively expects absorption is more pronounced for low-energetic antiprotons than for the high-energetic ones which have the opportunity to escape the high density zone earlier. Therefore, the finally observed spectrum is flatter than the original production spectrum.

Interestingly, while the baryon-baryon and the  $\rho\rho$  channels are comparable in their contribution to  $\bar{p}$  production, the pion-baryon channel turned out to be much more effective for all reasonable sets of parameters. This fact is indeed remarkable, because here, contrary to the discussion in Section II, the pions are not in chemical equilibrium; in our hadrochemical model the total time of the ignition phase is too short to saturate the pion channel. The meson-baryon channel is thus crucial for understanding  $\bar{p}$  spectra. Only by including all channels reliable predictions about the antiprotons can be drawn.

We did not mention so far that in our calculations we followed common practice and assumed a finite  $\bar{p}$  formation time of  $\tau = 1$  fm/c; this means that during this time interval

after a  $\bar{p}$ -producing collision the antiproton is assumed to be not yet fully developed and thus cannot annihilate. However, there are some (although controversial) experimental indications of an extremely long mean free path for antiprotons before final state interactions set in [26]. We have tested the influence of different values for the formation time  $\tau$  on the  $\bar{p}$  spectrum. Fig. 7 shows that this highly phenomenological and poorly established parameter has a very strong influence in particular on the absolute normalization of the spectra, i.e. the total production yield. In the light of this uncertainty it appears difficult to argue for or against the necessity for medium effects on the antiproton production threshold based on a comparison between theoretical and experimental total yields only.

### C. Comparison with Experimental Data

In all the calculations shown above a bombarding energy of 1 GeV/A has been assumed. Experimental data are, however, only available at around 2 GeV/A. At these higher energies thermalization becomes more questionable [27], and our simple model may be stretching its limits. Especially, the temperature in the fireball core becomes extremely high. In order to avoid such an unrealistic situation and in recognition of results from kinetic simulations [4,6,7] we thus assume that only part of the incoming energy is thermalized – in the following a fraction of 70% was taken.

Fig. 8 shows calculations for the antiproton spectrum from Na-Na and Ni-Ni collisions at a kinetic beam energy of 2 GeV/nucleon. The calculation assumes a  $\bar{p}$  formation time of  $\tau = 1$  fm/c, and takes for the density and temperature profiles the parameter value  $\alpha = 1$  which corresponds to an upside-down parabola for the density profile. Comparing with the GSI data [2] we see our model features too weak a dependence on the size of the collision system; the absolute order of magnitude of the antiproton spectrum is, however, correctly reproduced by our simple hadrochemical model, without adjusting any other parameters. No exotic processes for  $\bar{p}$  production are assumed. As mentioned in the previous subsection, the pion-baryon channel is responsible for getting enough antiprotons in our model, without

any need for a reduced effective  $\bar{p}$  mass in the hot and dense medium [4,5]. The existing data do not yet allow for a definite conclusion about the shape of the spectrum, and we hope that future experiments [28] will provide additional constraints for the model.

## V. CONCLUSIONS

Heavy ion collisions at typical BEVALAC and SIS energies are far below the  $p\bar{p}$ -production threshold. As a consequence, pre-equilibrium antiproton production in such collisions is strongly suppressed relative to production from the thermalized medium produced in the later stages of the collision. Therefore,  $\bar{p}$  production becomes important only when the heavy ion reaction is sufficiently far progressed, in accordance with microscopic simulations [4]. By assuming a local Maxwell-Boltzmann distribution for the scattered and produced particles forming the medium in the collision zone one maximizes the  $\bar{p}$  production rate (see Fig. 1). If, contrary to the assumptions made in this work, the extreme states in phase space described by the tails of the thermal Boltzmann distribution are not populated, the antiproton yield could be reduced substantially.

We also found that the threshold behaviour of the  $\bar{p}$  production cross section is not only crucial for the total  $\bar{p}$  yield, but also introduces structures into the initial  $\bar{p}$  spectrum. This might give rise to the hope that by measuring the  $\bar{p}$  momentum spectrum one may obtain further insight into the  $\bar{p}$  production mechanism. On the other hand we saw here, using a Fokker-Plank description for the later evolution of the distribution function  $f_{\bar{p}}(p, t)$  in a hot environment, that these structures are largely washed out by subsequent elastic scattering of the  $\bar{p}$  with the hadrons in the medium. In addition, the large annihilation rate reduces the number of observable antiprotons by roughly two orders of magnitude relative to the initial production spectrum; the exact magnitude of the absorption effect was found to depend sensitively on the choice of the  $\bar{p}$  formation time  $\tau$ .

We have also shown that meson (in particular pion) induced production channels contribute significantly to the final  $\bar{p}$  yield and should thus not be neglected. We were thus able

to reproduce the total yield of the measured antiprotons in a simple model for the reaction dynamics without including, for example, medium effects on the hadron masses and cross sections [4,5].

However, we must stress the strong sensitivity of the  $\bar{p}$  yield on various unknown parameters (e.g. the  $\bar{p}$  formation time) and on poorly controlled approximations (e.g. the degree of population of extreme corners in phase space by the particles in the collision region), and emphasize the rapidly thermalizing effects of elastic final state interactions on the  $\bar{p}$  momentum spectrum. We conclude that turning subthreshold antiproton production in heavy ion collisions into a quantitative probe for medium properties and collective dynamics in hot and dense nuclear matter remains a serious challenge.

#### ACKNOWLEDGMENTS

This work was supported by the Gesellschaft für Schwerionenforschung (GSI) and by the Bundesministerium für Bildung und Forschung (BMBF).

## REFERENCES

- [1] U. Mosel, *Annu. Rev. Nucl. Part. Sci.* 1991, Vol. 41, 29
- [2] A. Schröter *et al.*, *Z. Phys.* A350 (1994) 101
- [3] A. Shor *et al.*, *Phys. Rev. Lett.* 63 (1989) 2192
- [4] S. Teis, W. Cassing, T. Maruyama, and U. Mosel, *Phys. Rev.* C50 (1994) 388
- [5] G.Q. Li and C.M. Ko, *Phys. Rev.* C50 (1994) 1725
- [6] G. Batko *et al.*, *J. Phys.* G20 (1994) 461
- [7] C. Spieles *et al.*, *Mod. Phys. Lett.* A27 (1993) 2547
- [8] G.F. Bertsch and S. Das Gupta, *Phys. Rep.* 160 (1988) 189
- [9] P. Koch, B. Müller, and J. Rafelski, *Phys. Rep.* 42 (1986) 167
- [10] B. Schürmann, K. Hartmann, and H. Pirner, *Nucl. Phys.* A360 (1981) 435
- [11] G. Batko *et al.*, *Phys. Lett.* B256 (1991) 331
- [12] R.H. Milburn, *Rev. Mod. Phys.* 27 (1955) 1, and references therein
- [13] C.M. Ko and X. Ge, *Phys. Lett.* B 205 (1988) 195
- [14] P. Koch and C. Dover, *Phys. Rev.* C 40 (1989) 145
- [15] G. Feldman, *Phys. Rev.* 95 (1954) 1697
- [16] Landolt-Börnstein, *Numerical Data and Functional Relationships in Science and Technology*, Vol. 12a und Vol. 12b, Springer-Verlag Berlin, 1988
- [17] R. Wittmann, Ph. D. thesis, Univ. Regensburg, Feb. 1995
- [18] N.G. van Kampen, *Stochastic Processes in Physics and Chemistry*, North-Holland Publishing Company, Amsterdam 1983



- [19] B. Conforto *et al.*, *Nouvo Cim.* 54 A (1968) 441
- [20] W. Brückner *et al.*, *Phys. Lett. B* 166 (1986) 113
- [21] E. Eisenhandler *et al.*, *Nucl. Phys. B* 113 (1976) 1
- [22] S. Chandrasekhar, *Rev. Mod. Phys.* 15 (1943) 1
- [23] B. Svetitsky, *Phys. Rev. D* 37 (1988) 2484
- [24] I. Montvay and J. Zimanyi, *Nucl. Phys. A*316 (1979) 490
- [25] J.P. Bondorf, S.I.A. Garpman, and J. Zimányi, *Nucl. Phys. A*296 (1978) 320
- [26] A.O. Vaisenberg *et al.*, *JETP Lett.* 29 (1979) 661
- [27] A. Lang *et al.*, *Phys. Lett. B*245 (1990) 147
- [28] A. Gillitzer *et al.*, talk presented at the XXXIII International Winter Meeting on Nuclear Physics, 23.-28. January 1995, Bormio (Italy)

## FIGURES

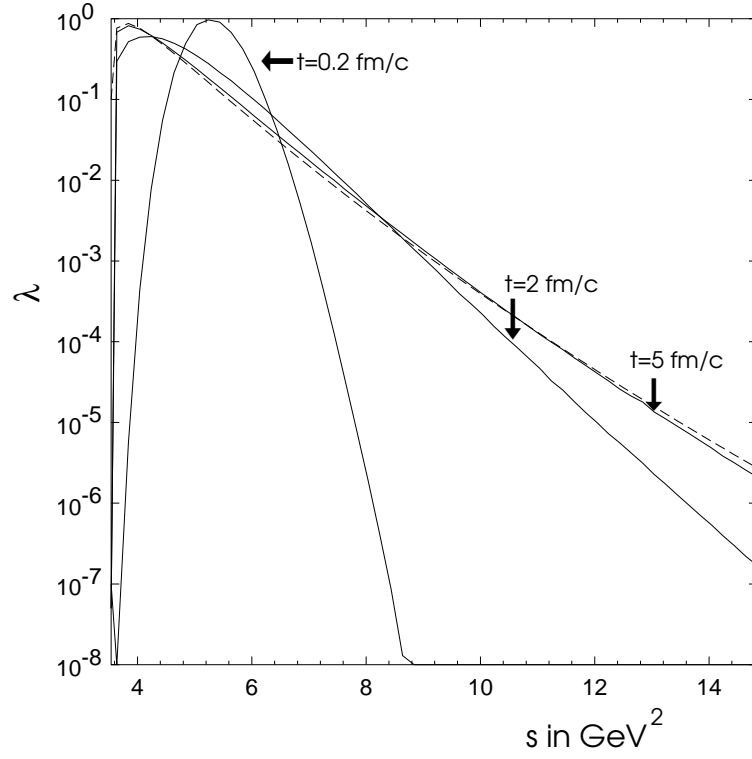


FIG. 1.  $\lambda(s, t)$  at different times  $t$  calculated from the model of Ref. [10]. The starting point is a  $\delta$ -function at  $s = 5.5 \text{ GeV}^2$ . The dashed line is the asymptotic thermal distribution at  $t = \infty$ , corresponding to a temperature  $T = 133 \text{ MeV}$ .

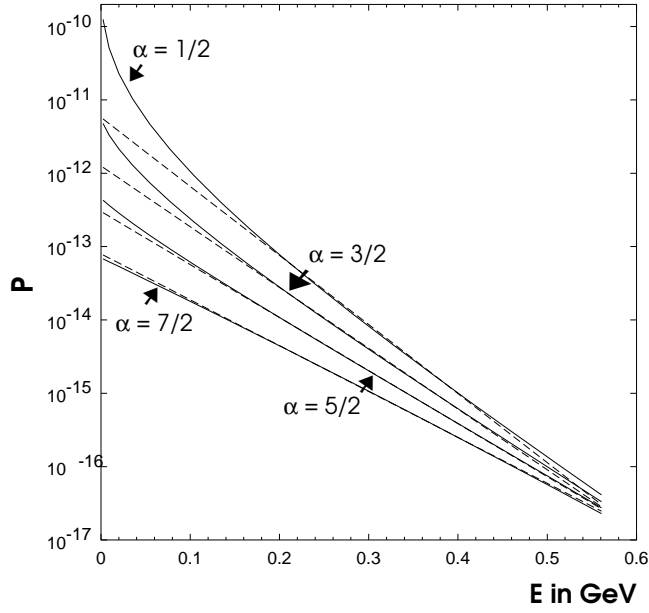


FIG. 2. Antiproton production spectrum for different threshold behaviour of the elementary production process ( $x = \frac{1}{2}, \frac{3}{2}, \frac{5}{2}, \frac{7}{2}$  from top to bottom).

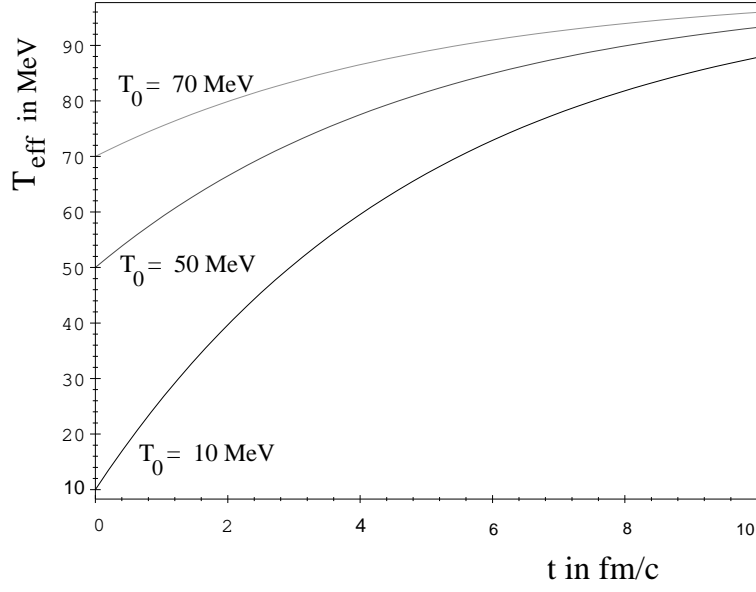


FIG. 3. Effective temperature  $T_{\text{eff}}$  for three Maxwell distributions with initial temperatures  $T_0 = 10$  MeV, 50 MeV and 70 MeV, respectively.

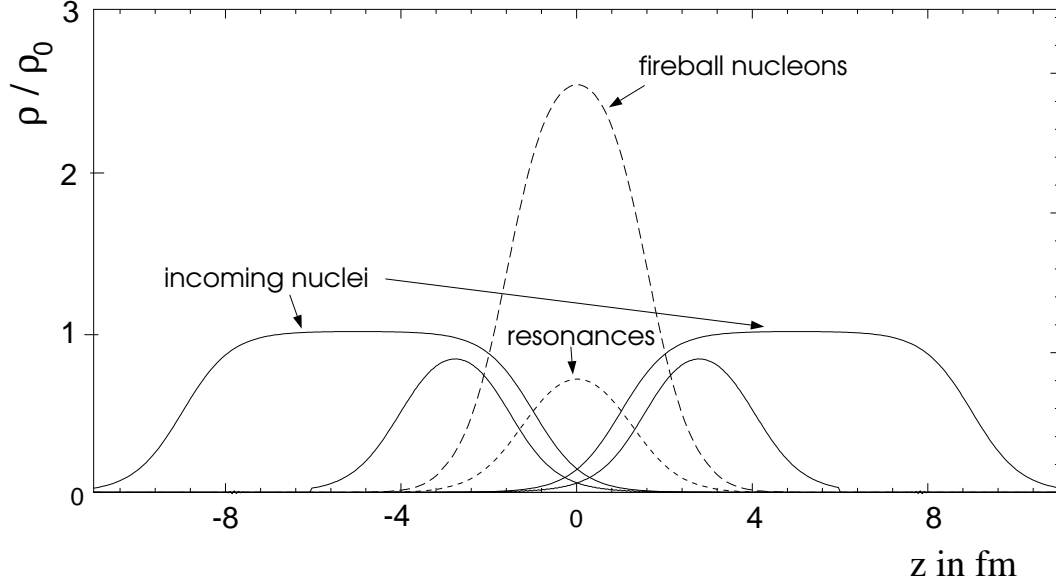


FIG. 4. Density distributions  $\rho(0,0,z)$  along the beam axis of target and projectile nucleons for a  $^{40}\text{Ca}$ - $^{40}\text{Ca}$  collision, normalized to  $\rho_0 = 0.15 \text{ fm}^{-3}$ . The solid lines labelled by “incoming nuclei” show the two nuclei centered at  $\pm 5$  fm at time  $t_0 = 0$ . The two other solid lines denote the cold nuclear remnants at full overlap time  $t_m$ , centered at about  $\pm 3$  fm. Also shown are fireball nucleons (long-dashed) and  $\Delta$ -resonances (short-dashed) at time  $t_m$ .

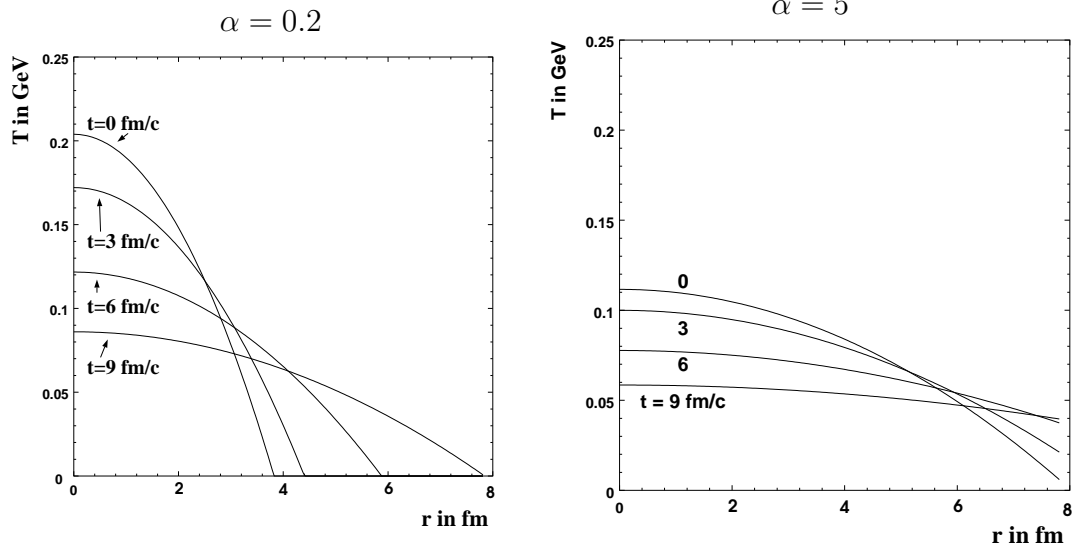


FIG. 5. Temperature profiles for  $\alpha = 0.2$  and  $\alpha = 5$  at four different times  $t = 0$  (=beginning of the explosion phase) and  $t = 3, 6,$  and  $9$  fm/c (from top to bottom).

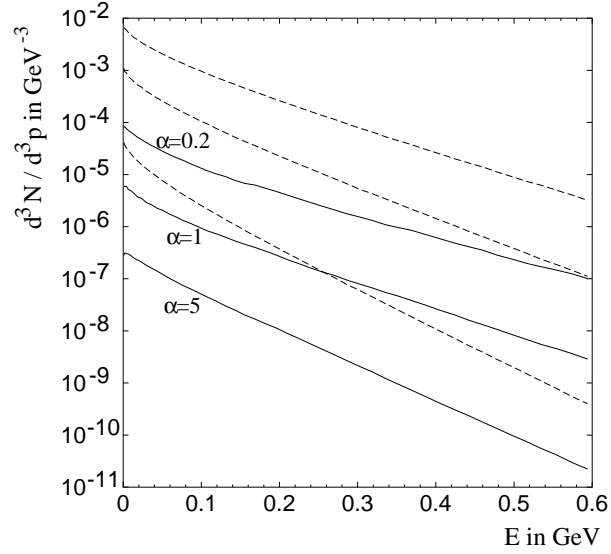


FIG. 6.  $\bar{p}$ -spectra for different profile parameters  $\alpha$ . The dotted lines mark the initial production spectra. The asymptotic temperatures at an assumed freeze-out density  $\rho_f = \rho_0/2$  corresponding to the solid lines are, from top to bottom, 105 MeV, 87 MeV and 64 MeV, respectively.

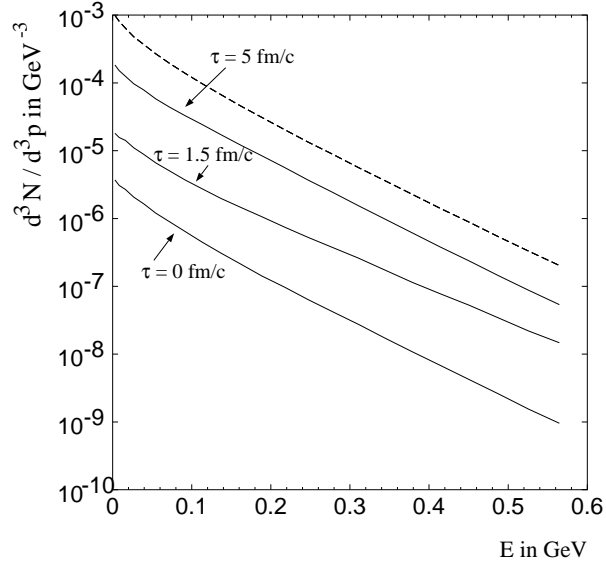


FIG. 7.  $\bar{p}$ -spectrum for different formation times, for a profile parameter  $\alpha = 1$ . The dashed line indicates the original production spectrum.



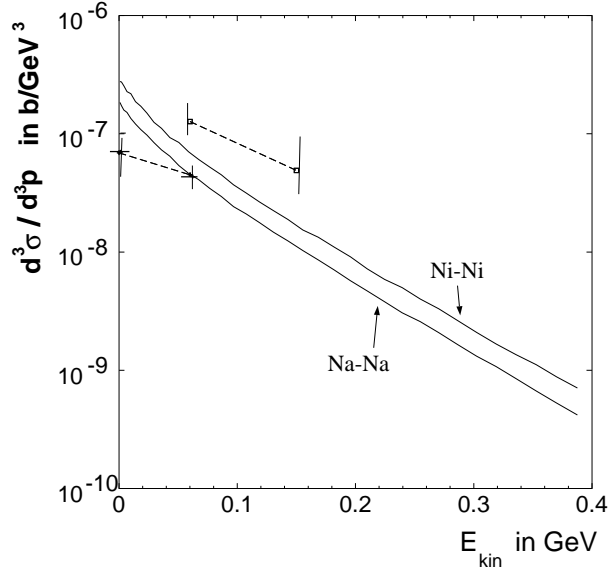


FIG. 8. Differential  $\bar{p}$  spectrum for Na-Na and Ni-Ni collisions, for a shape parameter  $\alpha = 1$ . The data are from GSI experiments [2].